Egypt. J. Chem. **Vol. 68**, No. 5 pp. 471 - 488 (2025)

Egyptian Journal of Chemistry

http://ejchem.journals.ekb.eg/

Theoretical Study of A Water Electrolyzer System for A Green Hydrogen Production Performance Evaluation Prediction

Hamdy H. El-Ghetany*[1], Mohamed A. Halawa[2], Aml E. Mohammed [2],

[1]*Solar Energy Department, National Research Centre, Dokki, 12622, Giza, Egypt*

[2]Mechanical Engineering Department, Al-Azhar University, Cairo, Egypt

Abstract

The main emphasis of the current study is to improve the performance of hydrogen (H_2) production under various working conditions via electrolysis of water. A mathematical model is designed and analysed considering the influence of several parameters such as electrolyte type, its concentration, electrode material with its surface area, number of electrolysis cells, generated thermal energy, applied pressure, temperature and current density. The system has been designed using Engineering Equation Solver (EES) Software. Results showed that the optimum cell voltage was achieved when the concentration of KOH solution as an electrolyte was 30% wt. On the other hand, the most suitable material for coating electrodes is iridium-dioxide (IrO_2) but its cost represented a challenge, stainless-steel can be used, alternatively, it is recommended to use substituted materials such as mixed metal oxides or non-precious metal catalysts. It was also found that the rate of the H_2 production and generated thermal energy increased as the surface area of the electrode plate, the number of cells, and current density were increased. the influence of increasing temperature on the cell voltage is studied, which causes the cell voltage to rise because of the ohmic resistance reduction, resulting lower operating cost. It is found that the cell voltage recorded 1.851 V at 40 °C, and 1.677 V at 80 °C. It is found that the operating pressure affects the reversible voltage, where a higher operating pressure leads to a non-linearly higher reversible voltage, resulting in a higher overall cell voltage.

Keywords: Green Hydrogen; Electrolysis; Alkaline Electrolyzer; Activation overpotential; Electrolyte Conductivity; Solar Energy.

1. Introduction

At the time being, the fossil fuel utilization has become a threat to the environment because it depletes the natural resources of the world [1-2]. Toward the global effort to minimize greenhouse gases, the use of clean energy sources is growing in that setting. Hydrogen gas is suggested to be used as an energy carrier within these sources, which enables for the combination of several sources of energy. This is why it becomes so important to create green hydrogen (GH_2) producing techniques [3]. However, hydrogen's chemical makeup prevents it from being kept in its pure form. It can be found in less energetic forms, such as those of hydrocarbons and water molecules [4]. As alkaline surroundings can be utilized for a variety of materials with satisfactory chemical properties under conditions of operation, alkaline water electrolysis is being a fundamental method that enables efficient storage and conversion of energy in light of the growing interest in energy from renewable sources and reducing carbon emissions from industry [5]. Besides, the main challenges in the electrolysis of water are reducing energy consumption, maintenance, and cost, also, increasing safety, durability, and reliability. Accordingly, a study on the production of H_2 electrically will be conducted [6]. In the alkaline electrolytic medium, the chemical bond between H_2 and oxygen (O_2) is broken by electrical energy generated by an electrolyzer, as a result, H_2 is separated from water molecules (H_2O). Inequality to steam and methane reforming, that gives H_2 along with carbon dioxide and carbon monoxide, electrolysis of water only gives H_2 and oxygen, with minimum emissions of greenhouse gases [7]. Equation (1) shows the basic chemical reaction of water electrolysis.

$$H_2O_{(l)} + \text{electric energy} \rightarrow H_{2(g)} + 0.5\ O_{2(g)} \quad (1)$$

Electrolyzer is a device that performs an electrolysis process. The electrolyzer has several advantages such as its efficiency reaching 70%, H_2 that produced from the electrolyzer is of high purity that requires little space, and contains few moving parts

*Corresponding author e-mail: hamdy.elghetany@gmail.com ; (Hamdy El-Ghetany).

Received date 13 August 2024; revised date 22 August 2024; accepted date 22 September 2024

DOI: 10.21608/ejchem.2024.312122.10190

[8]. A mathematical model has been developed using several input parameters. The ohmic over-potential, pressure, temperature, and activation over-potential represented the different parameters that the electrolyzer performance relied on. The model can be applied in order to predict the polarization behaviour when various input parameters will be changed. Results concluded that, the cell voltage of the electrolysis process decreased when the operational pressure decreased and the operational temperature increased. On the other hand, the ideal cell voltage was achieved when the KOH solution concentration was about 30 % wt. [9]. It has been investigated how different variables were affecting the efficiency of water electrolysis in producing H_2. According to these investigations, the ideal parameters for using the electrolysis might be achieved with a given solution concentration, electrode spacing, and input voltage [10]. On the other hand, the electrical current parameters have an effect on the efficiency of the electrolysis [11]. An uncomplicated model of an advanced electrolyzer for alkaline water has been studied utilizing the electrochemical equations and theoretical thermodynamic functions. the V/I characteristics calculation of the model has been illustrated as well as some parameters of the electrochemical process such as ohmic losses, activation potential and reversible potential. At 25 °C, a Ni-based electrodes in a single electrolysis cell has been used in order to verified the validity of real an experimental data Results showed that the model is applicable at 1 $A.cm^{-2}$ current density and at 80 °C [12]. The H_2 production potential produced from water electrolysis was evaluated in Cameroon using wind and solar renewable energies. Their simulation results showed that, for a wind turbine the hydrogen generation potential recorded 0.675 Nm^3/h, while for a solar energy recorded 0.55 Nm^3/h, which corresponds to around 84% and 70% average energy efficiency respectively [13]. Sea water is used to produce H_2 gas by the sea water electrolysis, and the effect of the type of electrode model is studied. Copper and graphite are used as electrodes type in the process of electrolysis at 12-volt potential difference. Results showed that, copper electrode is better than graphite in terms of life and durability. On the other hand, the produced H_2 from sea water electrolysis in the presence of graphite electrodes is much less than the H_2 produced in the presence of copper electrodes [14]. The performance of an "all-iron" electrolytic cell operating on economical steel electrodes steel is demonstrated. The alkaline water electrolyzer used a thin catalytic layer of alpha-nickel hydroxide to coat a steel mesh for the oxygen evolution electrode, while for the H_2 electrode, a nickel and molybdenum coating are used to coat another steel mesh. At 70 °C and 23 °C, the cell voltage of an electrolysis process is about 1.71 V and 1.83 V respectively and the current density is about 100 mA cm^{-2}. In that case, the KOH solution is 30 %wt. and the separator type is Zirfon. As the cell operation at 23 °C, and 100 mA cm^{-2} continuously for 100 h, the performance was no measurable loss. It is found that the electrodes based on iron are suitable for an electrolysis process [15]. El-Ghetany and El-Awady presented a theoretical analysis of designing a small-scale hydrogen generation unit containing two electrolyzers with 100 cells and 40 cm plate diameter to produce 75 kg H2 /day with consumed electric energy of 3360 kWh and 675 liter water/day, respectively. They presented also techno-economic study of the potential for green hydrogen production in Egypt. It is concluded that for designing a large-scale hydrogen generation plant with 280 ton/day (102,200 ton/year), the required electric power can be estimated as 618,333 kW (618.3 MW). Consequently; the electric energy consumption in MWh required can be estimated as 14,840 MWh and the required daily water consumed in m^3 /day can be estimated as 2,520m^3 /day. Other concluded remarks stated that the investment in green hydrogen production projects will be highly profitable as hydrogen can be sold as direct fuel, energy carrier or to be reacted with nitrogen to produce green ammonia where can be utilized as fertilizers and other useful industrial applications [16].

2. Modelling of Mathematical Equations

The polarization curve of an electrolyzer can be achieved using mathematical model according to several parameters. Empirical, thermodynamical, and electrochemical relationships are applied in order to obtain the mathematical model. In order to get the resulting cell voltage, various parameters affecting the electrolyzer performance are related to these equations.

2.1. Cell Voltage

For an alkaline electrolytic cell, the real voltage at which the electrolyze works is expressed as the cell voltage during the operational condition, the cell voltage takes into account all losses that occurring within the electrolyze cell. Equation (2) represents the total overpotential and reversible voltage occurring in the electrolyze which refers to the voltage of the cell [9].

$$V_c = V_{rev} + V_{act} + V_{ohmic} + V_{conc} \quad (2)$$

when current density is too extreme, concentration losses will be occurred. For this reason, the concentration effect of is neglected.

2.2. Reversible Voltage

The ideal voltage needed in order to begin the process of electrolysis is called open circuit voltage or reversible voltage. Nernst equation is the equation that describe reversible voltage and is depended on electrolysis pressure and temperature. But, the temperatures difference result in a reversible voltage variation, and in this regard, an additional term will be added to the Nernst equation to account this change and is given by equation (3)

$$V_{rev} = E^{\circ}_{rev} + (T - T_{ref}) * \frac{\Delta S^{\circ}}{nF} + \frac{RT}{2F}\left[\ln\left(\frac{(P-P_{H_2O})^{\frac{3}{2}}}{\frac{P_{H_2O}}{P^{\circ}_{H_2O}}}\right)\right] \quad (3)$$

For electrolysis process and at STP, equation (4) describes the lowest reversible voltage occurring [9].

$$E^{\circ}_{rev} = \frac{\Delta G^{\circ}}{2F} \quad (4)$$

Where:

ΔG°: Gibbs free energy variation and equation (5) describes it.

$$\Delta G^{\circ} = \Delta H^{\circ} - T_{ref}\Delta S^{\circ} \quad (5)$$

Equations (6) and (7) show the water vapor pressure above the electrolyte and the pure H_2O vapor pressure respectively [9].

$$\ln P_{H_2O} = 0.016214 - 0.13802m + 0.19330\sqrt{m} + 1.0239 \ln P^{\circ}_{H_2O} \quad (6)$$

$$P^{\circ}_{H_2O} = 37.043 - \frac{6275.7}{T} - 3.4159 \ln T \quad (7)$$

Where m is electrolyte molarity, that can be calculated by equation (8).

$$m = \frac{wt\%(183.1221 - 0.56845T + 984.5678 \exp(\frac{wt\%}{115.96277})}{5610.5} \quad (8)$$

Where wt.%: is the potassium hydroxide weight percentage.

2.3. Activation Over-Potential

The energy measurement needed to breakdown chemical bonds is called the activation over-potential. It is the electron transfer reaction kinetics occurring at the electrode reaction site. It is also a result of the excess voltage across the electrode. Equations (9) and (10) describe the activation voltages to activate the anode and cathode respectively, that is determined by the Tafel equation [9].

$$V_{act-a} = b_a \ln\left(\frac{j_a}{j_{o-a}}\right) \quad (9)$$

$$V_{act-c} = b_c \ln\left(\frac{j_c}{j_{o-c}}\right) \quad (10)$$

Equation (11) shows the Tafel slope for cathode and anode electrode [9].

$$b_{a,c} = \frac{RT}{nF\alpha_{a,c}} \quad (11)$$

The relationship between temperature and charge transfer coefficient ($\alpha_{a,c}$) for the Ni electrode is demonstrated in Equation (12) and (13) [17].

$$\alpha_a = 0.0675 + 0.00095T \quad (12)$$

$$\alpha_c = 0.1175 + 0.00095T \quad (13)$$

The exchange current density ($j_{o-a,c}$) is shown in Equation (14) [9].

$$j_{o-a,c} = \gamma_{a,c} * j_{o,ref-a,c} * \exp\left[\frac{-\Delta G_{c-a,c}}{R}\left(\frac{1}{T} - \frac{1}{T_{ref}}\right)\right] \quad (14)$$

The surface of the electrode contained bubbles, where the fractional coverage of bubbles (θ) is given by equation (15) [9].

$$\theta = \left(-97.25 + 182\frac{T}{T_{ref}} - 84\left(\frac{T}{T_{ref}}\right)^2\right)\left(\frac{j}{j_{lim}}\right)^{0.3}\frac{P}{P - P_{H_2O}} \quad (15)$$

Where:

j_{lim}: It is considered the limiting current density when the bubble coverage is equal to 100% [18].

In consequence, equation (16) indicates the activation overpotential involving bubble coverage [9].

$$V_{act-a,c} = b_{a,c} \ln\left(\frac{j_{a,c}}{j_{o-a,c}}\right) + b_{a,c} \ln\left(\frac{1}{1-\theta}\right) \quad (16)$$

2.4. Ohmic Overpotential

It is occurred in electrolytes, membranes, and electrodes electrical resistance. The sum of the individual resistances resulting from the electrolyte, membrane, and electrode is called the total ohmic resistance. Equation (17) expresses the ohmic overpotential [9].

$$V_{ohmic} = I\left(R_{ele} + R_{ely} + R_{mem}\right) \quad (17)$$

2.4.1. Electrode Resistance

The total electrical resistance resulting from cathode and anode electrodes is called the electrode resistance. The area, resistivity, and length of electrode material are the parameters on which the electrode resistivity depends as shown in equation (18) [9].

$$R_{a,c} = \rho_{eff-a,c}\frac{t_{a,c}}{A_{a,c}} \quad (18)$$

Equation (19) describes the electrode effective resistance.

$$\rho_{eff-a,c} = \frac{\rho_{o-a,c}}{(1-\epsilon_{e-a,c})^{\frac{3}{2}}} \quad (19)$$

The change in temperature leads to variation in electrodes material resistance with100% density, in order to compensate for this change in effective resistance, a new term is presented into equation (18) called the temperature coefficient of resistivity k_{a-c} as shown in equations (20-22).

$$R_{ele} = \rho_{eff-a}\frac{t_a}{A_a}[1 + K_a(T - T_{ref})] + \rho_{eff-c}\frac{t_c}{A_c}[1 + K_c(T - T_{ref})] \quad (20)$$

$$I = I_{density} * A_{ele} \quad (21)$$

$$A_{ele} = \left(\frac{\pi}{4}\right)D^2 \quad (22)$$

2.4.2. Electrolyte Resistance

The resistance that an electrolyte solution has is called electrolyte resistance. Another parameter that also acts on the electrolyte solution resistance is the bubble created. Equation (23) shows the total electrolyte solution resistance, which expresses the electrolytic resistance value in the presence and absence of the bubble [9].

$$R_{ely} = R_{ely-free} + R_{ely-bubble} \quad (23)$$

Equation (24) describes the electrolytic resistance in the presence of the bubble, which is the function of the electrolytic resistance in the absence of the bubble.

$$R_{ely-bubble} = R_{ely-free}\left(\frac{1}{\left(1-\frac{2}{3}\theta\right)^{\frac{3}{2}}} - 1\right) \quad)\quad (24)$$

Equation (25) describes the electrolytic resistance in the absence of the bubble

$$R_{ely-free} = \frac{1}{\sigma_{KOH-free}}\left(\frac{d_{am}}{A_a} + \frac{d_{cm}}{A_c}\right) \quad (25)$$

Equation (26) illustrates the ionic conductivity of potassium hydroxide [9].

$$\sigma_{KOH-free} = -2.04m - 0.0028m^2 + 0.005332mT + 207.2\frac{m}{T} + 0.001043m^3 - 0.0000003m^2T^2 \quad (26)$$

2.4.3. Membrane Resistance

In order to stop the gas mixing inside the electrolyzer, A separator or membrane must be placed between electrodes. The separator has a number of pores inside it, where the separator porosity (ε_m) is the volume fraction of these pores. Equation (27) shows the separator resistance to conduction of ions, which relies on separator physical properties [9].

$$R_m = \left(\frac{1}{\sigma_{KOH-free}}\right)\frac{\tau_m^2 t_m}{\omega_m \epsilon_m A_m} \quad (27)$$

2.5 Faraday Efficiency

At electrodes, the rate of electron transfer affects the H_2 production, according to faraday's law, which is proportional to the external circuit electrical current. Conversely, in the electrolyzer, the highest practical to theoretical volume of H_2 generated, is called Faraday's efficiency. In terms of temperature, the higher the temperature, the lower the resistance, the lower the Faraday's efficiency, and the higher the current losses, which can be showed by equation (28) [8].

$$\eta_F = \left[\left(\frac{I}{A_{ele}}\right)^2 / f_1 + \left(\frac{I}{A_{ele}}\right)^2\right] f_2 \quad (28)$$

Equation (29) determines the total rate of H_2 production in an electrolyzer containing many cells connected to each other in series [8].

$$\dot{n}H_2 = \eta_F \frac{N_{cell} I}{ZF} \quad (29)$$

The rate of production for water and oxygen consumption is shown in equation (30)

$$\dot{n}H_2o = \dot{n}H_2 = 2\dot{n}_{o_2} \quad (30)$$

The H_2 volume flow rate is shown in equation (31)[8]:

$$Q = \dot{n}H_2 * 3600 * 0.022414 \quad (31)$$

The generated thermal energy is shown in equation (32) [8]:

$$Q_{gen} = N_{cell} * I * (V_{cell} - V_{tn}) \quad (32)$$

Thermoneutral Voltage (Per Cell) is given by equation (33) [8]:

$$V_{tn} = \frac{\Delta H}{Z*F} \quad (33)$$

The current mathematical model is developed using the EES software. Table 1 demonstrates the constant parameters needed for the model [9, 19, 20].

2.6 Specific Electrolyte Conductivity

Equations (34, 35) show the specific electrolyte conductivities for potassium hydroxide and sodium hydroxide respectively [22]. Equation (34) belongs to the mass fraction of potassium hydroxide (W_{KOH}) between 0.15 and 0.45 and the temperature T (K) extending from 258.15 to 373.15K, while equation (35) is appropriate for the mass fraction of sodium hydroxide (W_{NaOH}) between 0.08 to 0.25 and the temperatures θ (°C) extending from 25 to 50 °C. Table 2 shows the parameters required to compute these conductivities [21] [22].

$$\sigma_{KOH} = K_1(100.W_{KOH}) + K_2.T_{KOH} + K_3.T_{KOH}{}^2 + K_4.T_{KOH}(100.W_{KOH}) + K_5.T_{KOH}^2(100.W_{KOH})^{K_6} + K_7\frac{T_{KOH}}{(100.W_{KOH})} + K_8\frac{(100.W_{KOH})}{T_{KOH}} \quad (34)$$

$$\sigma_{NaOH} = K_1 + K_2.T_{NaOH} + K_3.W_{NaOH}^3 + K_4.W_{NaOH}^2 + K_5.W_{NaOH} \quad (35)$$

2.7 Equations for Electrode Material

The ohmic overpotential is produced by the voltage whose conductivity is in the range of 10 $mScm^{-1}$, where the of stainless-steel or titanium electrodes conductivity is about 2.5 $kScm^{-1}$. In this regard, the ohmic overpotential given in equation (36) [24] is:

$$U_{ohm} = \frac{\delta_m i_{cell}}{\sigma_m} \quad (36)$$

The Butler–Volmer equation describes the activation overpotential in equation (37) [23,24]:

$$U_{act} = \frac{RT_{el}}{\alpha_{an}F}\operatorname{arcsinh}\left(\frac{i_{cell}}{2i_{o,an}}\right) + \frac{RT_{el}}{\alpha_{cat}F}\operatorname{arcsinh}\left(\frac{i_{cell}}{2i_{o,cat}}\right) \quad (37)$$

Table 1: Electrolyer Constant Parameters [9, 18, 19].

Constants	Symbols	Values	Unit
Reference Temperature	T_{ref}	298	K
Standard Entropy Change	ΔS°	-162.86	J/mol.K
Number of electrons	n	2	-
Faraday Constant	F	96485	C/mol.
Universal Gas Constant	R	8.315	J/mol.K
Standard Enthalpy Change	ΔH°	-286.02	Kj/mol
Weight Percent of KOH Solution	wt %	30	%
Electrode Roughness Factor Anode	γ_a	1.25	-
Electrode Roughness Factor Cathode	γ_c	1.05	-
Free Energy of Activation Anode	ΔG_a	41500	J/mol.K
Free Energy of Activation Cathode	ΔG_c	23450	J/mol.K
Reference Exchange Current Density Anode	$j_{o,ref-a}$	$1.34535*10^{-5}$	A/cm^2
Reference Exchange Current Density Cathode	$j_{o,ref-c}$	$1.8456*10^{-3}$	A/cm^2
Surface Area of Anode and Cathode	A_a, A_c	300	cm^2
Surface Area of Membrane	A_m	300	cm^2
Thickness of Anode and Cathode Electrode	t_a, t_c	0.2	cm
Thickness of Membrane	t_m	0.05	cm
Resistivity of the 100%-Dense NI Electrode	ρ_a, ρ_c	$6.4*10^{-6}$	Ω cm
Temperature Coefficient of Resistivity	k_a, k_c	0.00586	$/^0C$
Distance Between Anode and Membrane	d_{am}	0.125	cm
Distance Between Cathode and Membrane	d_{cm}	0.125	cm
Porosity of Anode	ϵ_a	0.3	-
Porosity of Cathode	ϵ_c	0.3	-
Porosity of Membrane	ϵ_m	0.42	-
Tortuosity of Membrane	τ_m	2.18	-
Wettability Factor	ω_m	0.85	-
Limiting current Density at 100 % bubble coverage	j_{lim}	30	A/cm^2

Exchange current densities and charge transfers coefficients are demonstrated in [23,25]. Equation (38) describes the cell voltage basic model [24]:

$$U_{cell} = U_{rev} + \frac{\delta_m i_{cell}}{\sigma_m} + \alpha \text{arcsinh}\left(\frac{i_{cell}}{2i_o}\right) \quad (38)$$

Table 2: Specific conductivities parameters special for KOH and NaOH solutions [21, 22]

Parameter	Equation (31)	Unit	Equation (32)	Unit
K_1	27.9844803	Sm^{-1}	-45.7	Sm^{-1}
K_2	-0.924129482	$Sm^{-1}K^{-1}$	1.02	$Sm^{-1}{}^0C^{-1}$
K_3	-0.0149660371	$Sm^{-1}K^{-2}$	3200	Sm^{-1}
K_4	-0.0905209551	$Sm^{-1}K^{-1}$	-2990	Sm^{-1}
K_5	0.0114933252	$Sm^{-1}K^{-2}$	784	Sm^{-1}
K_6	0.1765	-	-	-
K_7	6.96648518	$Sm^{-1}K^{-1}$	-	-
K_8	-2898.15658	$Sm^{-1}K$	-	-

3. Results and Discussion

3.1 Electrolyte Concentration Effectiveness

The potassium hydroxide and sodium hydroxide specific conductivity are determined based on equations (34) and (35), and according to the value of parameters listed in table 2. Figure 1 shows the specific conductivity at temperatures of 25 and 50°C, and the concentration of electrolyte will be taken into account.

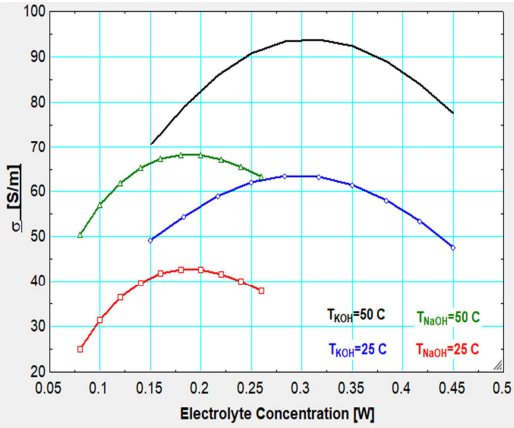

Figure 1: Specific conductivity of KOH and NaOH solutions depending on the solution concentration.

Results in figure 1 showed that the potassium hydroxide specific conductivity is greater than the sodium hydroxide specific conductivity. In fact, the potassium hydroxide specific conductivity is more favorable at temperatures between 50 and 80°C and for mass fractions of 25 and 35 wt.% as illustrated in [21,26]. The specific conductivity of sodium hydroxide solution is most suitable for mass fractions of 15 and 25 wt.%.

Figure 2(a) and 2(b) show the theoretical results of the KOH and NaOH specific conductivities for mass fractions of 15 and 25 wt.%, and at temperature between -20 and 100 °C. Results showed that the higher the temperature, the higher the conductivity. As shown in figure 2, KOH conductivity is 95 $S.m^{-1}$ at 50 °C, and 25 wt.%, while that of NaOH is 65 $S.m^{-1}$. On the other hand, at 25 °C, and 25 wt.%, the KOH specific conductivity is 63 $S.m^{-1}$, while that of NaOH is 41 $S.m^{-1}$. It can be concluded that, with decreasing temperature, the specific conductivity decreased.

3.2 Effect of Reversible, Activation and Ohmic voltages

Regarding the reversible voltage, theoretical results showed that at any value of concentration, pressure, and temperature, the reversible voltage is constant. On the other hand, when the cell requires energy for starting reactions at anode and cathode, a voltage drop will appear on both sides, therefore, activation losses take place.

Figure 3 showed the current density versus activation voltage at different operating temperatures. It can be observed from the result, the activation overpotential increased rapidly at low current density, leading to higher cell voltage. But, the activation overpotential increased slowly, with increasing current density.

From another side, the activation overpotentials are not affected by temperature variations. The ohmic overpotential was initially ignored because its value is minimal as it depends on current and resistance, but higher current density affects the ohmic overpotential, causing the curves of polarization to shift to higher voltage levels.

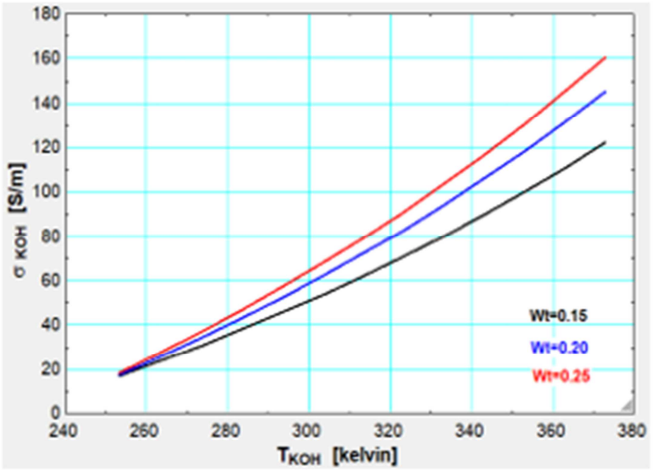

Figure 2 (a): Temperature of electrolyte versus KOH specific conductivity variation at 15, 20, and 25 wt %.

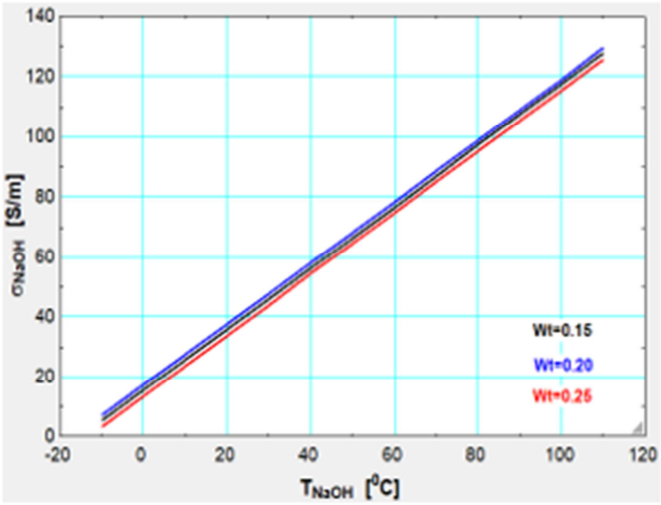

Figure 2 (b): Temperature of electrolyte versus NaOH specific conductivity variation at 15, 20, and 25 wt %.

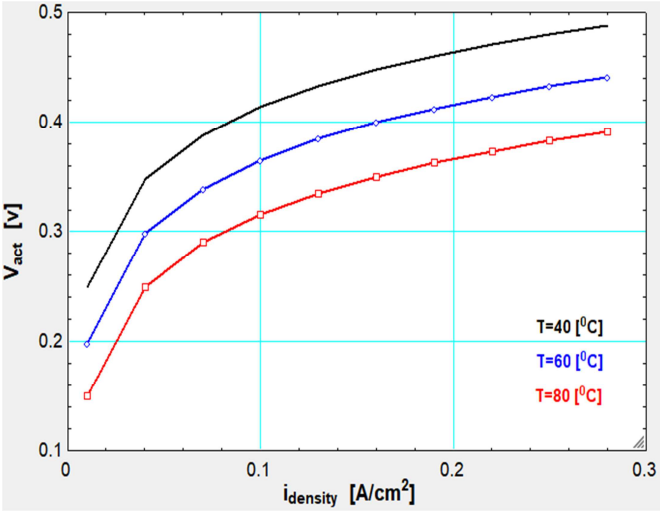

Figure 3: Current density versus activation voltage at different operating temperatures

Figure 4 shows the current density versus ohmic voltage at different operating temperatures. It can be observed that, the interfacial resistance of the electronic components increases when the current density increases, resulting in a higher ohmic overvoltage. On the other hand, the ohmic overpotentials is not affected by temperature changes when the current density is low, but when the current density increases with temperature variations, the ohmic overpotential characteristics exhibit a divergent performance. In summary, when the current densities are the same, ohmic overpotential is less than the activation overpotential. As can be seen from the result, when current density has 0.28 (A/cm^2) and temperature has 40 ^{o}C, the ohmic overvoltage is equal to 0.1009V, and the activation over-potentials is equal to 0.4882V.

3.3 Effect of Temperature on Cell Voltage

It is known that, at high voltage, molecules of water separate into O_2 and H_2 ions in case of increasing current density, and thus, it is clear from figure 5 that increasing current density leads to a corresponding rise in cell voltage at 7 bar and 30 W_{KOH} %. On the other hand, the influence of increasing temperature on the cell voltage is taken into account, which causes the cell voltage to rise because of the ohmic resistance reduction, resulting lower operating cost. From figure 5, the cell voltage recorded 1.851 V at 40 °C, and 1.677 V at 80 °C, which represent the largest and smallest value of the cell voltage respectively.

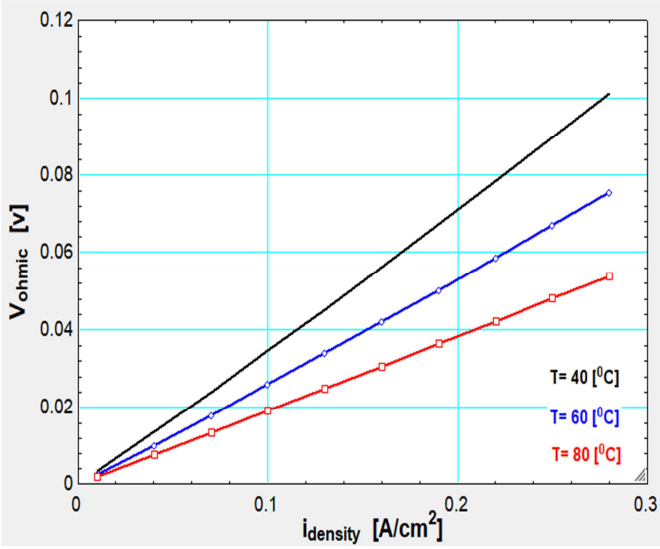

Figure 4: Current density versus ohmic voltage at different operating temperatures

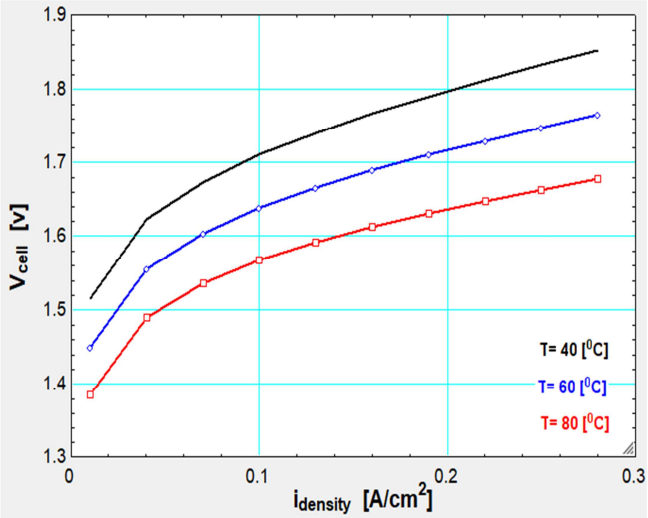

Figure 5: Variation of cell voltage vs current density at different temperatures at 7 bar and 30 w_{KOH}%.

3.4 Effect of Pressure on Cell Voltage

The operating pressure affects the reversible voltage as shown in figure 6, where a higher operating pressure leads to a non-linearly higher reversible voltage, resulting in a higher overall cell voltage. From another side, a decrease in the bubble coverage factor occurs at higher operating pressure, resulting in a decrease in resistance of electrolyte and activation overpotential.

3.5 Effect of Concentration

The electrolyte conductivity is affected by the KOH concentration, and as a result, the ohmic overpotential also affected. The KOH solution conductivity reaches its peak at 30 W_{KOH}%, if this solution concentration value moves up or down, it causes a decrease in the KOH conductivity, and thus the resistivity rises [21]. Figure 7 showed the concentration percentage versus on various resistances.

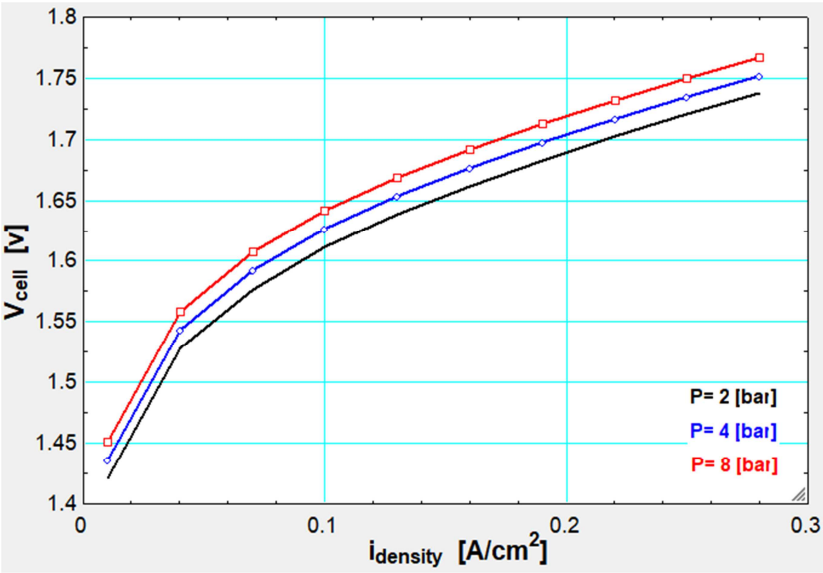

Figure 6: Current density versus cell voltage at different pressure value with 30 W_{KOH} % and 60 ^{o}C.

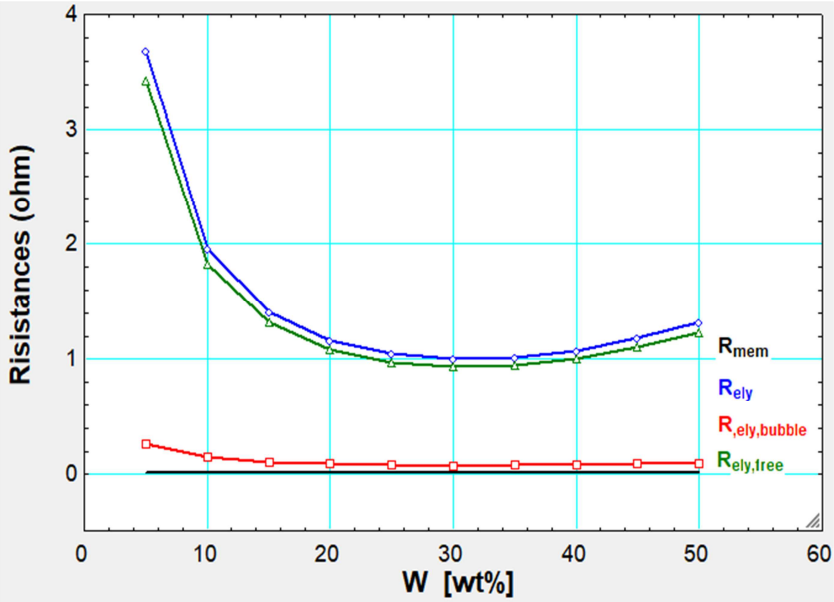

Figure 7: Concentration percentage versus R_{mem}, R_{ely}, $R_{ely\text{-}free}$, $R_{ely\text{-}bubble}$.

3.6 Effect of Number of Cells

The effect of current density on the volume flowrate of H_2 production is shown in figure 8. It can be seen that the value of volume flow rate of H_2 production gradually rises with increasing current density. Furthermore, the influence of the cell number on the volume flow rate of H_2 production was demonstrated, where the volume flowrate characteristics of H_2 production at higher current densities showed divergent performance depending on the cell number. Figure 9 demonstrated the cell number effect on the volume flow rate of H_2 production. It can be noted that, the larger number of cells causes a larger flow rate of H_2 production. In addition, the volume flowrate of hydrogen production increases with increasing the current density.

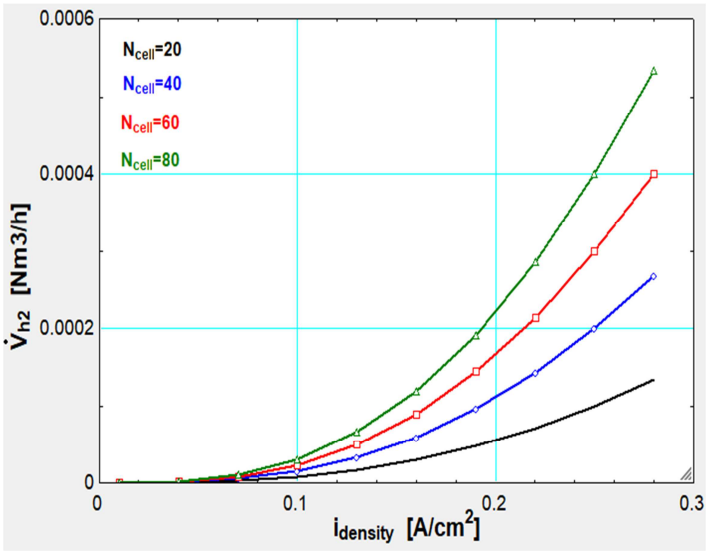

Figure 8: Current density versus volume of H_2 production rate at various number of cells.

3.7 Effect of Electrolyte's Temperature

Figure 10 presented an obviously influence of temperature on reversible voltage, activation over-potential and ohmic overpotential.

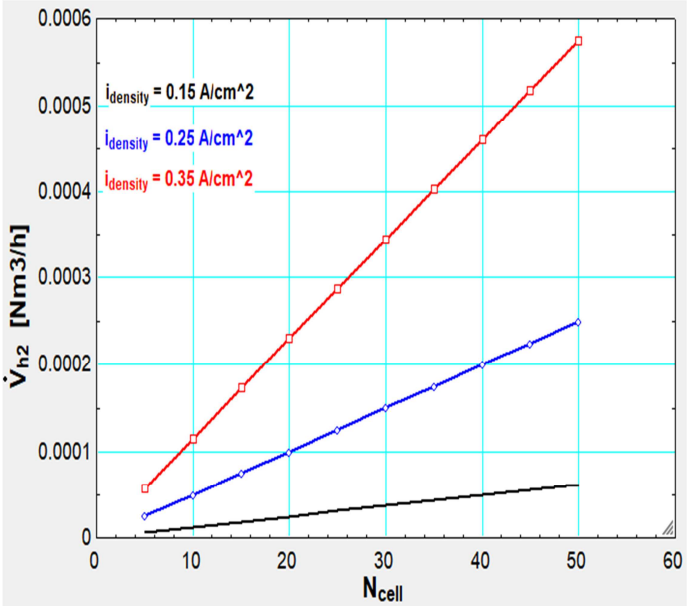

Figure 9: Number of cells versus volume flow rate of H_2 at various current densities

Results showed that, when there is an increase in the temperature from 20 ^oC to 120 ^oC, the reversible voltage drops by 0.076 V from 1.464 V to 1.388 V, which has a greater effect on the reversible voltage. As for the activation over-potential, it drops by 0.067 V from 1.178 V to 1.111 V, and drops by 0.003431 V from 0.0115 V to 0.008069 V for the ohmic over-potential, which has the least effect on ohmic overpotential. The of temperature influence on the cell voltage is shown in figure 11 at different current densities. Results showed that, at low temperature, the cell voltage is very high and gradually decreases with increasing temperature. As shown in figure 11, the cell voltage drops by 0.176 V from 2.653 V to 2.507 V at 150 mA/cm^2 current density, and when the temperature rises from 0 ^oC to 120 ^oC. Furthermore, figure 12 shows the pressure versus electrolyte temperature. Obviously, as the temperature increases, the pressure increases.

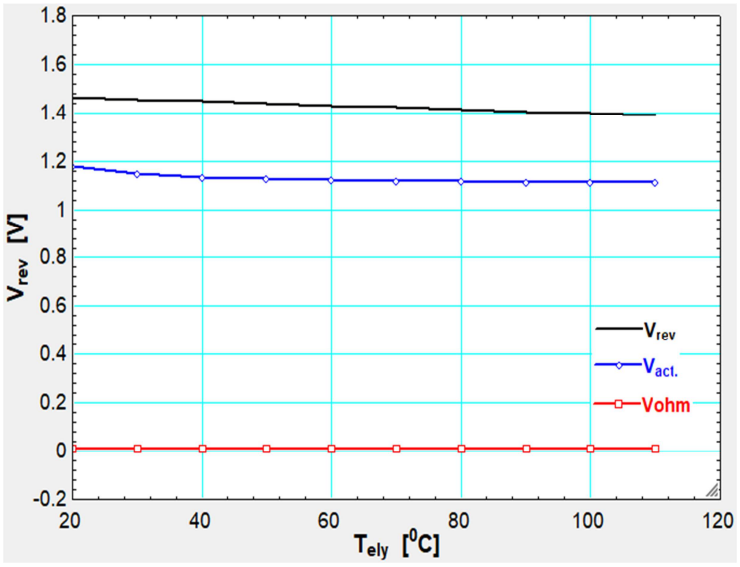

Figure 10: Influence of electrolyte temperature on Vrev., Vact, Vohm

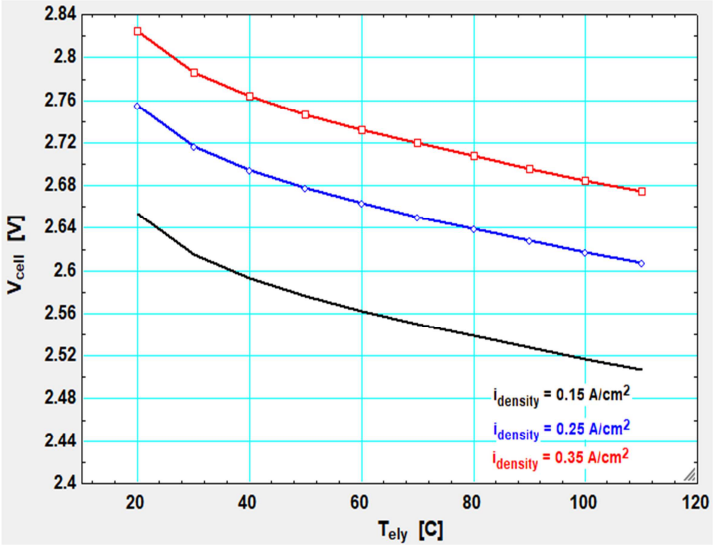

Figure 11: Cell voltage versus electrolyte temperature at various current densities

3.8 Generated Thermal Energy

Figure 13 shows the Number of cells versus generated thermal energy at various current densities. Results demonstrated that, the generated thermal energy will be higher with increasing the number of cells and current densities. Furthermore, figure 14 shows the volume flow rate of H_2 production versus the generated thermal energy at various current densities. Results show that with the increase of the volume flow rate of H_2 production and current density, the generated thermal energy increases.

3.9 Electrode Surface Area

The effect of plate surface area on the H_2 production rate for different cell numbers is shown in figures 15 and 16. It is clear that, increasing the current density with increasing plate surface area leads to a higher H_2 production rate with increasing the plate diameter and number of cells. Figure 15 showed that, at plate diameter of 1m and 80 cells, the H_2 production rate is 5.094 Nm^3/h. Similarly, as shown in figure 16, at a plate surface area of $1m^2$ and 80 cells, the H_2 production rate is 5.305 Nm^3/h.

3.10 Electrode Material

The widely material used for electrodes is the stainless steel according to its high corrosion resistance and minimum cost. The distances between the cathode and anode from 3 mm to 16 mm for obtaining the V-I characteristics of the electrolyze cell [24]. Results showed that, as the electrode distance increases, the current density decreases.

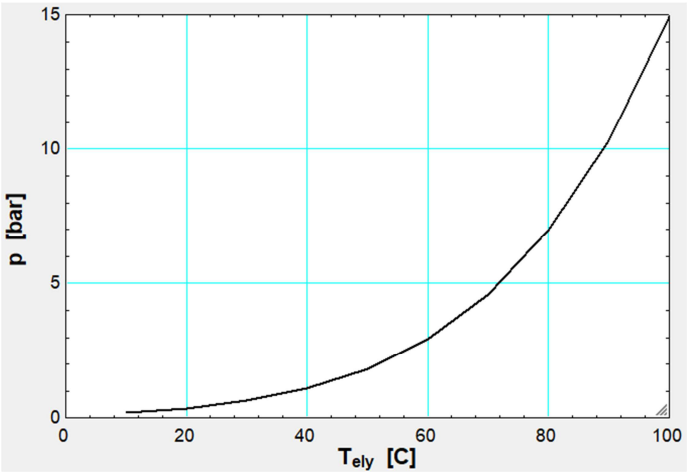

Figure 12: Pressure versus electrolyte temperature.

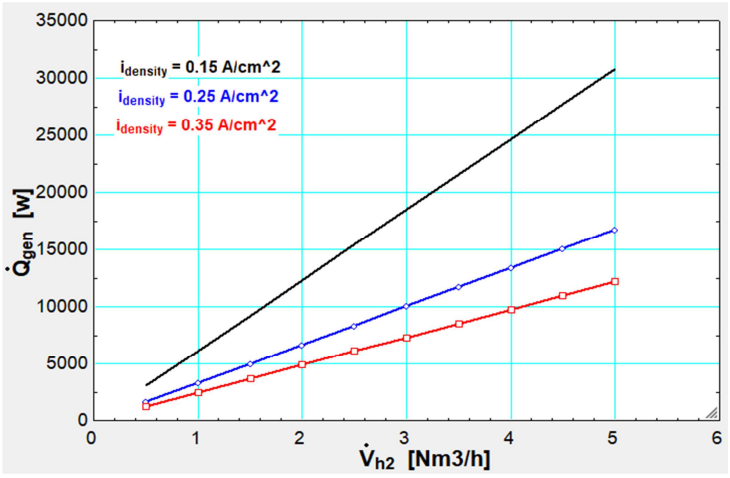

Figure 13: Number of cells versus generated thermal energy at various current densities

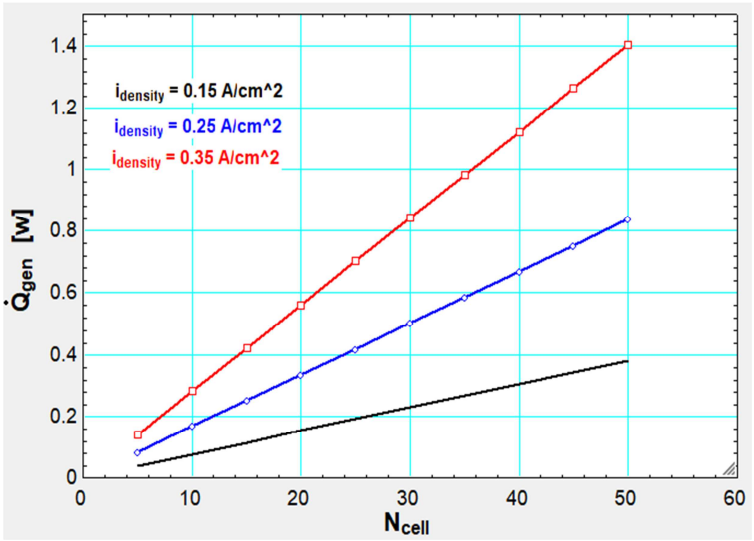

Figure 14: Volume flow rate of H_2 production versus generated thermal energy at various current densities

Consequently, in order to improve the efficiency, it is vitally important to minimize the electrode distance. Various types of electrode materials are displayed, like iridium dioxide (IrO2), platinum (Pt), graphite (C), nickel (Ni), and stainless steel (SS). In each test, the anode and cathode were coated with the same type of material in order to observe which one of these materials gives the best performance. Figure 17 showed the effect of electrodes type on the voltage of the cell, where parameters of the model are given in table 2 according to [24].

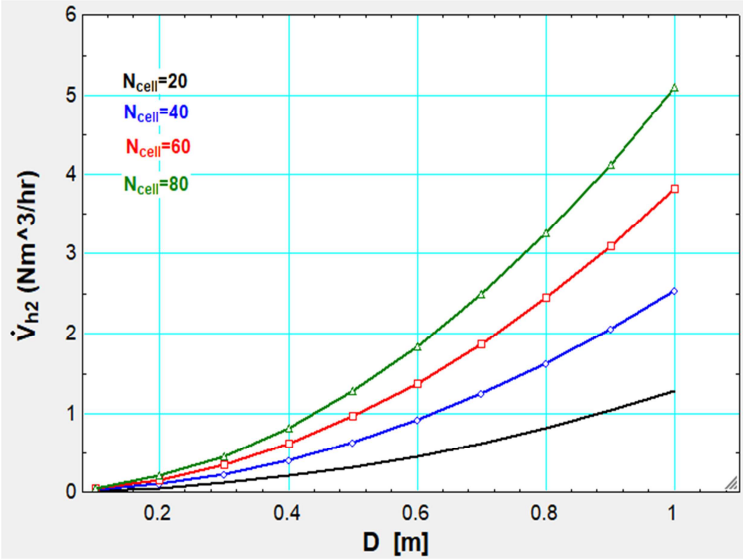

Figure 15: Electrode diameter vs H_2 volume flow rate in (Nm^3/h).

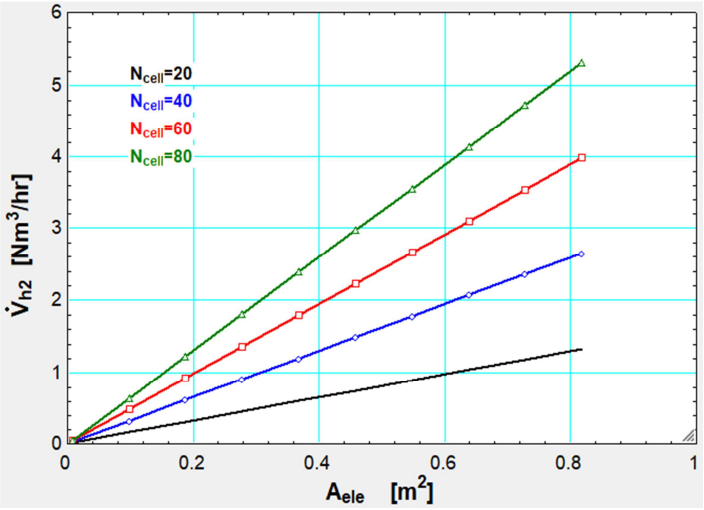

Figure 16: Electrode surface area vs H_2 volume flow rate in (Nm^3/h).

Figure 17 shows that, the electrode coated with iridium-dioxide is clearly the most suitable type, as it gives the lowest cell voltage, followed by platinum type. The electrodes coated with stainless-steel and nickel have relatively close voltage. Finally, it is clear that graphite has a bad effectiveness, as the cell voltage is very high.

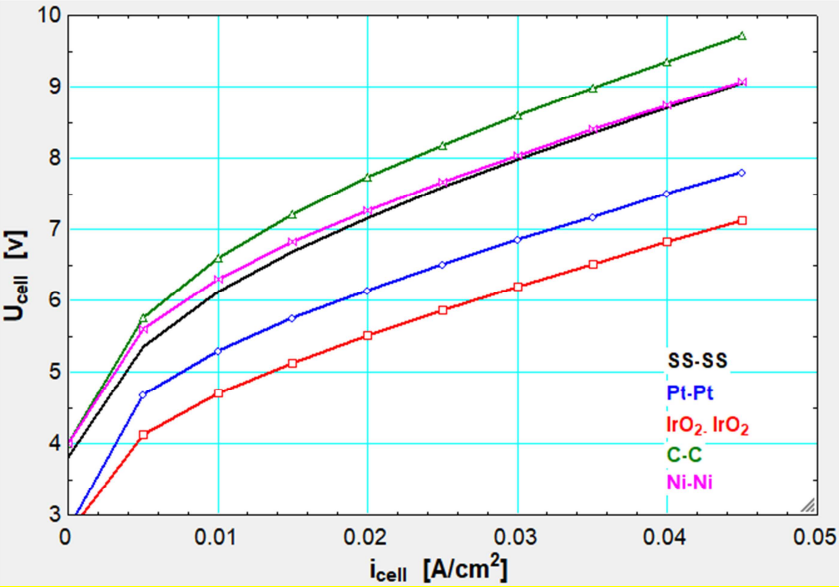

Figure 17: Effect of electrodes type on the voltage of the cell.

Table 3: Cell model Parameters with different types of electrode materials

An/Cat	U_{rev} (v)	σ_m (s cm^{-1})	α	i_o (A cm^{-1})
Pt-Pt	1.4	0.012	0.255	0.0002
Iro_2- Iro_2	1.366	0.012	0.227	0.0004
SS-SS	1.905	0.012	0.393	0.0010
C-C	2	0.012	0.455	0.0010
Ni-Ni	2	0.012	0.338	0.0007

4. Conclusion

A mathematical model for alkaline water electrolysis was developed using several input parameters by means of EES software, and the polarization curve was generated. Results concluded that, in order to lowering the cell voltage as much as possible, and thus increase the efficiency of the electrolyzer, it may be possible to raise the cell operating temperature and reduce the operating pressure. From another point of view, potassium hydroxide solution is more suitable than sodium hydroxide solution as an electrolyte because its specific conductivity is higher. In addition, the best cell performance occurs when the KOH solution has a concentration of about 30 wt%. On the other hand, the influence of cells number, electrode surface area, and electrode material on the electrolyzer performance were taken into account. Concerning with the electrode spacing, it should to be as low as possible to reach the low cell voltage and achieve a high efficiency. It is also found that the electrode coated with iridium-dioxide is clearly the most suitable type, as it gives the lowest cell voltage. Higher H_2 production rate is achieved by increasing the plate diameter, plate surface area and number of cells. The generated thermal energy will increase with larger cell number, current density, and H_2 production rate.

5. Nomenclatures

A_a	Anode surface area, cm^2
A_c	Cathode surface area, cm^2
A_m	Area of membrane, cm^2
$A_{a,c}$	Cross-sectional area of anode and cathode
A_{ele}	Area of electrode, cm^2
b_a	Anode Tafel's coefficients for, V
$b_{a,c}$	Tafel slope

b_c	Cathode Tafel's coefficients for, V
D	Diameter of electrode, m
d_{am}	Gap between membrane and anode, cm
d_{cm}	Gap between membrane and cathode, cm
E°_{rev}	At STP, V, it represents the lowest reversible voltage needed to start the electrolysis process.
F	Faraday Constant, C/mol
f_1	Faraday Efficiency Parameter, mA/cm^4
f_2	Faraday Efficiency Parameter
I	Current, A
$I_{density}$	Current Density, A/cm^2
i_o	Exchange current density on the electrode surfaces, A/cm
$j_{a,c}$	Anode and Cathode current density for, A/cm^2
i_{cell}	Electrode material current density for, A/cm^2
j_{lim}	Limiting current density at 100% bubble coverage, A/cm^2
$j_{o-a,c}$	Effective exchange current density, A/cm^2
$j_{o,ref-a,c}$	Reference exchange current density at temperature T_{ref},
K_a	Temperature coefficient of resistivity for anode, C^{-1}
K_c	Temperature coefficient of resistivity for cathode, C^{-1}
m	Molarity of the electrolyte
N_{cell}	Number of cells
$\dot{n}H_2$	Hydrogen production rate, Nm^3/h
$\dot{n}H_2o$	Production rate for water
n	number of electrons
$\dot{n}_{o_2}$	Oxygen production rate
P	Operational pressure, bar
P_{H_2O}	The vaporized water pressure across the electrolyte, bar
$P^{\circ}_{H_2O}$	Vapor pressure of pure H_2O, bar
Q	Volume flow rate of H_2, Nm^3/h
Q_{gen}	Generated thermal energy, W
R	Universal gas constant, J/mol K
$R_{a,c}$	Electrode resistance, ohm
R_{ele}	Resistance due to electrode, ohm
R_{ely}	Resistance due to electrolyte, ohm
$R_{ely-bubble}$	Electrolyte solution resistance containing bubble, ohm
$R_{ely-free}$	Electrolyte solution resistance without bubble, ohm
R_{mem}	Resistance due to membrane, ohm
R_T	Thermal resistance, K/W
T	Operating temperature, K
t_a	Anode thickness, cm
t_c	Cathode thickness, cm
T_{el}	Temperature of electrolyzer used for electrode material, K
T_{KOH}	Temperature of potassium hydroxide solution, K
t_m	Membrane thickness, cm
T_{NaOH}	Temperature of sodium hydroxide solution, ^0C
T_{ref}	Reference temperature at which E°_{rev} and ΔS° is evaluated, K
U_{act}	Activation overpotential used for electrode material, V
U_c	Cell voltage used for electrode material, V
U_{ohmic}	Ohmic overvoltage used for electrode material, V
$U_{rev,a,c}$	Reversible voltage used for electrode material, V
V_{act}	Activation overpotential, V
V_c	Cell voltage, V
V_{conc}	Concentration overvoltage, V
V_{ohmic}	Ohmic overvoltage, V

V_{rev}	Reversible voltage, V
V_{tn}	Thermo-neutral voltage, V
W	Electrolyte concentration, wt%
W_{KOH}	Potassium hydroxide concentration, wt%
W_{NaOH}	Sodium hydroxide concentration, wt%
Z	Number of electrons
$\alpha_{a,c}$	Anode and Cathode charge transfer coefficient
$\Delta G_{c-a,c}$	Free energy of activation, J/mol K
ΔS°	Change in entropy at T_{ref}, J/mol K
$\frac{\Delta S^{\circ}}{nF}$	Standard state entropy changes at 25° C.
ΔH°	Change in enthalpy at T_{ref}
δm	Distance between the electrodes, cm
$\epsilon_{e-a,c}$	Porosity of the electrode
ϵ_m	Porosity of the membrane
η_F	Faraday's efficiency
$\rho_{a,c}$	Electrode resistivity of the, Ωm
$\rho_{eff-a,c}$	Electrode effective resistance, Ωm
$\rho_{o-a,c}$	Resistivity of the 100%-dense anode, cathode material Ωm
τ_m	Tortuosity of membrane
$t_{a,c}$	Anode and Cathode the thickness
θ	Fractional bubble coverage (θ) on the electrode surface
$\sigma_{KOH-free}$	Bubble-free ionic conductivity of KOH solution, S/m
σ_m	Conductivity of the medium, S/cm
σ_{NaOH}	Electrical conductivity of sodium hydroxide, S/m
σ_{kOH}	Specific electrolyte conductivity for potassium hydroxide, S/m
$\gamma_{a,c}$	Electrode roughness factor of electrode
ω_m	Wettability of membrane

6. Conflicts of interest

The authors declare that they have no conflicts of interest regarding this article.

7. Formatting of funding sources

The authors did not receive any funding.

8. References

[1] Winter, C. J., "Hydrogen Energy - Abundant, Efficient, Clean: A debate over the energy-system-of-change", International Journal of Hydrogen Energy, vol. 34, no. 14, suppl. 1, pp. 1-52,2009.DOI:10.1016/j.ijhydene.2009.03.003.

[2] Chakik, F. E., Kaddami, M., Mikou, M., "Optimization of physico-chemical parameters of hydrogen production by electrolysis of water", IEEE Xplore 2018 Renewable Energies, Power Systems & Green Inclusive Economy (REPS-GIE),2018.DOI:10.1109/REPSGIE.2018.8488777

[3] Vigoya, M. F., Mendoza, J. O. G., Abril, S. O., "Development and simulation of an electrolytic cell for hydrogen generation", Journal of Xi'an University of Architecture & Technology, vol. 12,no.7,pp.45-56, 2020. DOI :10.1234 /jxuat .2020.1207.

[4] Sun, C. W., Hsiau, S. S., "Effect of Electrolyte Concentration Difference on Hydrogen Production during PEM Electrolysis", Journal of Electrochemical Science and Technology, vol. 9, no. 2, pp. 99-108, 2018. DOI: 10.5229/JECST.2018.9.2.99.

[5] Ďurovič, M., Hnát, J., Bouzek, K., "Electrocatalysts for the hydrogen evolution reaction in alkaline and neutral media. A comparative review", Journal of Power Sources, vol. 493, art. no. 229708, 2021. DOI: 10.1016/j.jpowsour.2021.229708.

[6] Yuvaraja, A. L., Santhanaraj, D., "A Systematic Study on Electrolytic Production of Hydrogen Gas by Using Graphite as Electrode", *Materials Research*, vol. 17, no. 1, pp. 83-87, 2014. DOI: 10.1590/S1516-14392013005000153.

[7] Abomazid, A. M., "Modeling and Control of Electrolysis Based Hydrogen Production System", Graduate Program in Electrical Engineering and Computer Science, York University, Master Thesis, November 2021.

[8] Tijani, A. S., Yusup, N. A. B., Rahim, A. H., "A Mathematical Modelling and Simulation Analysis of Advanced Alkaline Electrolyzer System for Hydrogen Production", *Procedia Technology*, vol. 15, pp. 798–806, 2014. DOI: 10.1016/j.protcy.2014.09.053.

[9] Niroula, S., Chaudhary, C., Subedi, A., Thapa, B. S., "Parametric Modelling and Optimization of Alkaline Electrolyzer for the Production of Green Hydrogen", *IOP Conference Series: Materials Science and Engineering*, vol. 1279, art. no. 012005, 2023. DOI: 10.1088/1757-899X/1279/1/012005.

[10] Balabel, A., Zaky, M. S., Sakr, I., "Optimum Operating Conditions for Alkaline Water Electrolysis Coupled with Solar PV Energy System", *Arabian Journal for Science and Engineering*, vol. 39, pp. 4211–4220, 2014. DOI: 10.1007/s13369-014-0967-8

[11] Dobó, Z., Palotás, Á. B., "Impact of the current fluctuation on the efficiency of Alkaline Water Electrolysis", International Journal of Hydrogen Energy, vol. 42, pp. 5649–5656, 2017. DOI: 10.1016/j.ijhydene.2017.01.048.

[12] Borisov, G., Borisov, N., Petkucheva, E., Slavcheva, E., "Mathematical modeling and experimental validation of advanced alkaline water electrolyser U/j performance", *Proceedings of the Bulgarian Academy of Sciences*, vol. 52, Special Issue E, pp. 84–87, 2020. DOI: 10.7546/CEEP.2020.052.E84.

[13] Nkanga, E. R. E., Ndoh, D. Z., Ntonda, J., Nanfak, A., Mekouebe, M. T., Lontsi, F., "Modeling of Hydrogen Production in an Alkaline Electrolyser System Connected with a Solar Photovoltaic Panel or a Wind Turbine, Douala-Cameroon", *Journal of Power and Energy Engineering*, vol. 9, pp. 1-18, 2021. DOI: 10.4236/jpee.2021.910001.

[14] Rustana, C. E., Sunaryo, Salam, I. N., Sugihartono, I., Sasmitaningsihhiadayah, W., Madjid, A. D. R., Hananto, F. S., "Preliminary Study on The Effect of Time on Hydrogen Production from Electrolysis of the Seawater", Journal of Physics: Conference Series, vol. 1624, no. 1, art. no. 012095, 2021. DOI: 10.1088/1742-6596/2019/1/012095.

[15] Zayat, B., Mitra, D., Narayanan, S. R., "Inexpensive and Efficient Alkaline Water Electrolyzer with Robust Steel-Based Electrodes", Journal of The Electrochemical Society, vol. 167, no. 1, pp. 014508, 2020. DOI: 10.1149/1945-7111/aba792.

[16] H. H. El-Ghetany and M. H. El-Awady, Techno-Economic Study of the Potential for Green Hydrogen Production in Egypt, Egypt. J. Chem. Vol. 66, No. SI: 13 pp. 127-135 (2023), DOI 10.21608/EJCHEM.2023.188736.7493

[17] Hammoudi, M., Henao, C., Agbossou, K., Dubé, Y., Doumbia, M. L., "New multi-physics approach for modelling and design of alkaline electrolyzers", *International Journal of Hydrogen Energy*, vol. 37, no. 15, pp. 13895–13913,2012.DOI:10.1016/j.ijhydene.2012.07.015.

[18] Vogt, H., Balzer, R. J., "The bubble coverage of gas-evolving electrodes in stagnant electrolytes", *Electrochimica Acta*, vol. 50, no. 22, pp. 4449–4456,2005.DOI:10.1016/j.electacta.2005.05.01.

[19] Abdin, Z., Webb, C. J., Gray, E. M., "A Modelling and Simulation of an Alkaline Electrolyser Cell", *Energy*, vol. 139, pp. 797–805, 2017. DOI: 10.1016/j.energy.2017.08.031

[20] Rodríguez, J., Amores, E., "Modeling and experimental validation of an alkaline water electrolysis cell for hydrogen production", *Processes*, vol. 8, no. 12, pp. 1–17, 2020. DOI: 10.3390/pr8121634.

[21] Brauns, J., Turek, T., "Alkaline Water Electrolysis Powered by Renewable Energy: A Review", Processes, vol. 8, no. 2, pp. 248, 2020. DOI: 10.3390/pr8020248.

[22] Gambou, F., Guilbert, D., Zasadzinski, M., Rafaralahy, H., "A comprehensive survey of alkaline electrolyzer modeling: electrical domain and specific electrolyte conductivity", Energies, vol. 15, no. x, 2022. DOI:10.3390/en15093452.

[23] Larminie, J., Dicks, A., *Fuel Cell Systems Explained*, John Wiley & Sons Ltd., England, 2003.

[24] Givirovskiy, G., Ruuskanen, V., Ojala, L. S., Lienemann, M., Kokkonen, P., Ahola, J., "Electrode material studies and cell voltage characteristics of the in situ water electrolysis performed in a pH-neutral electrolyte in bioelectrochemical system", *Heliyon*, vol. 5, no. 2, art. no. e01690, 2019. DOI: 10.1016/j.heliyon.2019.e01690.

[25] Biaku, C., Dale, N., Mann, M., Salehfar, H., Peters, A., Han, T., "A semiempirical study of the temperature dependence of the anode charge transfer coefficient of a 6kW PEM electrolyzer", *International Journal of Hydrogen Energy*, vol. 33, no. 16, pp. 4247–4254, 2008. DOI: 10.1016/j.ijhydene.2008.06.006.

[26] Brauns, J., Schönebeck, J., Kraglund, M. R., Aili, D., Hnát, J., Žitka, J., Mues, W., Jensen, J. O., Bouzek, K., Turek, T., "Evaluation of Diaphragms and Membranes as Separators for Alkaline Water Electrolysis", *Journal of The Electrochemical Society*, vol. 168, no. 1, art. no. 014510, 2021. DOI: 10.1149/1945-7111/abda57.